Electromechanical Modeling of a Permanent-Magnet Spherical Actuator Based on Magnetic-Dipole-Moment Principle

Chee Kian Lim, I-Ming Chen, *Senior Member, IEEE*, Liang Yan, *Member, IEEE*, Guilin Yang, *Member, IEEE*, and Kok-Meng Lee, *Fellow, IEEE*

***Abstract*—Theoretical modeling in any engineering design is of paramount importance as it establishes the interrelationship between variables being analyzed in a given condition. With regard to the design of a permanent-magnet spherical actuator, electromechanical modeling is crucial as it correlates the input parameters such as current to the output mechanical torque. In this paper, a new approach in electromechanical-torque formulation for this class of spherical actuator employing the magnetic-dipole-moment principle is being discussed. Derivation from first principle and the extension of this novel method in the acquisition of the 3-D resultant torque induced on the rotor are presented. The proposed approach circumvents the need for electromagnetic-energy analysis within the air gap between the rotor and stator poles and, henceforth, providing a direct computation of the resultant torque. The validity of the proposed analytical torque model was verified against numerical and empirical data. Comparisons between the 3-D torque results demonstrate the correctness and soundness of the proposed electromechanical torque model.**

***Index Terms*—Electromechanical torque modeling, magnetic-dipole-moment principle, permanent-magnet (PM) spherical actuator.**

I. Introduction

MULTIDEGREES-OF-FREEDOM (DOF) actuators or motors are favored over conventional systems, particularly in robotics applications. Demands for multi-DOF manipulators have since motivated researchers to explore various aspects in terms of mechanical design and actuation methods. The key objective was to have an efficient and, ideally, a direct-drive configuration that provides multi-DOF motions. By encompassing multi-DOF motions excluding the presence of auxiliary systems not only enhances the system dynamic response but also improves structural rigidity and avoids workspace singularities. The history of multi-DOF actuator, or motor, dates back to the mid-1950s. The first spherical induction motor was designed and constructed by Williams *et al.* [1] from the University of Manchester, U.K. Joining in the foray in the design for such versatile actuators ignites the interests of many researchers all over the world [2]–[16]. Various forms and configurations in the structural design for spherical actuators were conceived to date. In order to achieve multi-DOF motion, a diverse array of operating principle were considered, spanning from utilizing mechanical technique [9], electromechanical options [6], and to the much preferred electromagnetic-induction approach [1]–[5], [7], [8], [10]–[12].

From the brief introduction earlier, one would concur that an electromagnetic actuation scheme is the choice of many designs as it avoids direct contact between the moving and stationary parts of the actuator. Moreover, single-DOF electromagnetic induction motors are a well-established field in terms of mechanical design and theoretical formulations [17]–[20]. Regrettably, for the electromechanical analysis of multi-DOF spherical electromagnetic actuators remains a teething issue arising from its 3-D workspace and nonlinear properties of ferromagnetic material [3], [5], [14]. Complexity involved in the analysis of such an electromechanical system hinders the implementation of real-time control. For this reason, control of some existing prototypes is confined to commutation scheme [5], [8], [11] where the rotor steps upon each actuation. This has significantly clipped the full potential of such actuators. Hence, in order to achieve continuous isotropic real-time motion control of an electromagnetic spherical actuator, a viable analytical torque model that establishes the relationship between input current and the output torque is critical.

There are various approaches one can undertake for the torque analysis of such class of actuators. These methods include the coenergy or virtual-work method [5], Maxwell stress-tensor approach [2], [3], [14], and the Lorentz force law [7], [10], [16]. The coenergy or virtual-work method analyzes the mechanical output by evaluating the magnetic potential energy of the system. In a magnetostatic field where dissipation mechanisms are absent, the stored energy in the field equals to the energy required to create it. Hence, the force or torque imparted to the magnetized body can therefore be computed. For this method, it is greatly hindered by the intricacy involved during the formulation of the energy density function in 3-D space. In addition, fluctuating field variation in space and flux leakages poses even more challenges for this technique. Lorentz force

Manuscript received April 29, 2008; revised October 23, 2008. First published November 18, 2008; current version published April 29, 2009. This work was supported by a collaborative research project under Grant U02-A-O40B for Nanyang Technological University, Singapore Institute of Manufacturing Technology, and Georgia Institute of Technology.

C. K. Lim, I-M. Chen, and L. Yan are with the School of Mechanical and Aerospace Engineering, Nanyang Technological University, Singapore 637098 (e-mail: limck@pmail.ntu.edu.sg; michen@ntu.edu.sg; yanliang@pmail.ntu.edu.sg).

G. Yang is with the Mechatronics Group, Singapore Institute of Manufacturing Technology, Singapore 638075 (e-mail: glyang@simtech.a-star.edu.sg).

K.-M. Lee is with the George W. Woodruff School of Mechanical Engineering, Georgia Institute of Technology, Atlanta, GA 30332-0405 USA (e-mail: kokmeng.lee@me.gatech.edu).

Color versions of one or more of the figures in this paper are available online at http://ieeexplore.ieee.org.

Digital Object Identifier 10.1109/TIE.2008.2009526

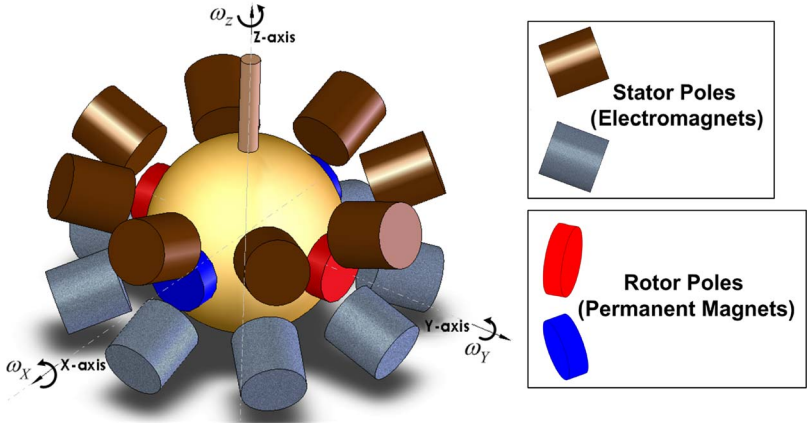

Fig. 1. Spherical actuator prototype and its working principle.

law governs the electromechanical interaction between moving charge and fields, and Maxwell stress tensor deals with the force density function. In these two methods, the prerequisite will be the knowledge of magnetic-field distribution in the region of interest and, hence, circumvent the inclusion of magnetic-energy function. The downsides to these two schemes lie in the need to acquire complete magnetic-field distribution within the region of interest and to perform full integration along the path of the moving charge. For these reasons, Lorentz force-law or the Maxwell stress-tensor approach can be computationally exhaustive for real-time control implementation. Although analytical solutions can be established, it is still a step from ideal.

In this paper, we are proposing a new approach based on the magnetic-dipole-moment principle in acquiring the output torque of the permanent-magnet (PM) spherical actuator. The proposed model is able to overcome the shortcomings of the existing electromechanical methods discussed earlier. The main advantages of this novel approach as compared to others are as follows.

1) Complete magnetic-flux-density $\mathbf{B}$-field description of the system is not necessary. Only spatial point in the region of interest is required.
2) Vectorial approach in torque computation as compared to conventional integration approach.
3) Able to establish and correlate the input and output parameters analytically.

With the aforementioned attributes, computation time for the resultant torque of the spherical actuator can be significantly reduced. With this new technique coupled with the analytical magnetic-field model developed [15], a complete electromechanical model can be formulated and computed. The model also correlates and establishes the input and output parameters of the electromechanical system for subsequent design optimization and control. The ensuing sections will present the minutiae of the PM spherical actuator and the newly proposed electromechanical model.

II. PM Spherical Actuator

In most electromagnetic setups, the magnetic circuits consist of field sources such as magnets or coils with the utilization of ferromagnetic materials, guiding the path of the magnetic flux. The advantage of such configuration is the higher power-to-torque ratio but at the expense of a complex control scheme largely due to the inherent presence of detent forces, hysteresis, saturation, and nonlinear characteristics of the ferromagnetic materials. Therefore, in order to realize a dexterous multi-DOF spherical actuator for positioning application, it would be ideal if the system possesses a linear relationship between the input and the output parameters. For this reason, the PM spherical actuator was proposed as shown in Fig. 1. The main difference of this prototype as compared to others will be the absence of ferromagnetic material within the system, resulting in a linear correlation between the input current and the output torque.

The spherical actuator possesses three rotational DOFs. To better understand how 3-D motion is generated, we can envision it from the schematic working principle shown in Fig. 1. From the fundamental universal law of like poles repelling and unlike poles attracting each other, rotary and directional control can be achieved by the manipulation of the electromagnets input current. Extending the earlier working principle by arranging PMs around the surface of the rotor and distributing electromagnets surrounding the spherical surface, we are able to realize the 3-D motion as desired.

III. Proposed Electromechanical Model

A. Magnetic-Dipole-Moment Principle

For an arbitrary current distribution, vector potential $\mathbf{A}(\mathbf{x})$ has multipole expansion in the order of dipole, quadrupole, octopole terms, etc., except the monopole term. For the asymptotic analysis, the dominant term at large distances is the dipole term. The vector potential is given by

$$\mathbf{A}(\mathbf{x}) = \frac{\mu_0}{4\pi} \int \frac{\mathbf{J}(\mathbf{x}')d^3x'}{|\mathbf{x}-\mathbf{x}'|} \tag{1}$$

where $\mathbf{J}(\mathbf{x}')$ is the current density at the source point. The magnetic dipole moment of a current distribution can be defined by

$$\mathbf{m} = \frac{1}{2} \int \mathbf{x}' \times \mathbf{J}(\mathbf{x}')d^3x'. \tag{2}$$

The dipole moment $\mathbf{m}$ is an intrinsic property of the current distribution that does not depend on the observation point $\mathbf{x}$.

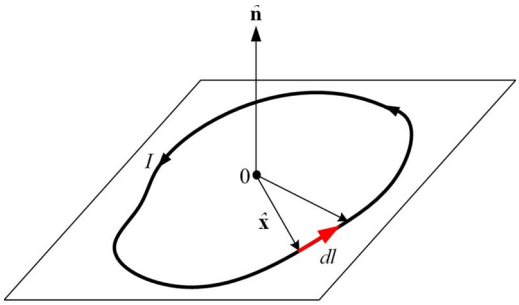

Fig. 2. Planar current loop.

Extending to the case of a planar current loop C with current I, we recall that $\mathbf{J}(\mathbf{x}')d^3x'$ is the same as Idl for current in a wire. The shape of the wire is irrelevant as long as it is planar. We may picture this wire loop carrying the current as shown in Fig. 2. Therefore, by replacing the parameters, we have the dipole moment of a wire loop as

$$\mathbf{m} = I \oint_C \frac{1}{2}\mathbf{x}' \times dl. \tag{3}$$

The vector $1/2x' \times dl$ is perpendicular to the plane of the loop with the magnitude equal to the area of the infinitesimal triangular sector bounded by $\mathbf{x}'$, $\mathbf{x}' + dl$, and dl. Thus,

$$\mathbf{m} = IA\hat{\mathbf{n}} \tag{4}$$

where $\hat{\mathbf{n}}$ is the normal unit vector and A is the area of the loop. In order to formulate an electromechanical model for the spherical actuator based on the magnetic-dipole phenomenon, it is essential to consider the dynamics of the dipole itself. The key relationship which we want to establish will be the force or torque effect by an external field $\mathbf{B}$ on the dipole. Considering the case of a planar current loop, the torque on the planar loop due to the magnetic forces on current distribution can be expressed by

$$N = \oint_C \mathbf{x} \times d\,\mathbf{F} = \oint_C \mathbf{x} \times (Id\,\mathbf{x} \times B) \tag{5}$$

where $d\mathbf{x}$ is an infinitesimal segment of the curve at $\mathbf{x}$. If $\mathbf{B}$ field is assumed to be uniform and constant in the region of the current, by cross product identity

$$d\left[\mathbf{x} \times (\mathbf{x} \times \mathbf{B})\right] = \mathbf{x} \times (d\,\mathbf{x} \times \mathbf{B}) + d\,\mathbf{x} \times (\mathbf{x} \times \mathbf{B}).$$

Since the start and end points of the integration are the same for a loop, we will have the loop integral equals to zero. Inferring from earlier, the remaining two terms on the right-hand side are equal but opposite. Therefore, we may write

$$N = \frac{I}{2} \oint_C \left[\mathbf{x} \times (d\,\mathbf{x} \times \mathbf{B}) - d\,\mathbf{x} \times (\mathbf{x} \times \mathbf{B})\right].$$

Given that $\mathbf{a} \times (\mathbf{b} \times \mathbf{c}) + \mathbf{b} \times (\mathbf{c} \times \mathbf{a}) + \mathbf{c} \times (\mathrm{a} + \mathbf{b}) = 0$, we rewrite N as

$$N = \frac{I}{2} \oint_C \left[(\mathbf{x} \times d\,\mathbf{x}) \times \mathbf{B}\right] = \mathbf{m} \times \mathbf{B} \tag{6}$$

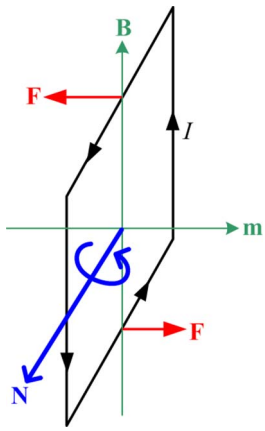

Fig. 3. Torque on a planar loop.

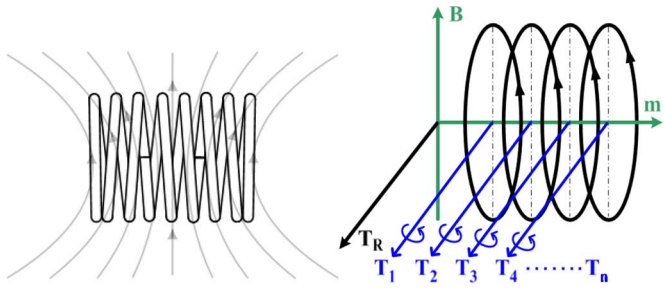

Fig. 4. Superposition of resultant torque of a solenoid.

with $\mathbf{m}$ defined by (4). The result earlier reveals that the torque on a magnetic dipole is perpendicular to $\mathbf{B}$ in the direction twisting the dipole moment $\mathbf{m}$ toward the alignment with the $\mathbf{B}$ field. This result is applicable to any pointlike magnetic dipole. To gain some intuition, Fig. 3 shows (6) pictorially. The orientation potential energy associated with this torque can be derived from a mechanical argument.

A natural occurrence illustrating the magnetic-dipole-moment phenomenon can be observed from a magnetized needle put through a cork floating on the surface of water. Due to the Earth's magnetic field and the aforementioned torque, the needle becomes aligned with the field pointing north. From earlier, we have shown that a current loop under the influence of an external $\mathbf{B}$ field will experience a magnetic moment about its normal as prescribed by (6). Hence, by extending this phenomenon to a solenoid consisting of a series of current loops, by superposition principle, we can resolve the resultant torque through the summation of the individual loops as shown in Fig. 4.

B. Electromechanical Model for PM Spherical Actuator

Applying the preceding notion to our specific application, the objective is to evaluate the torque acting on the rotor when the stator coils are being energized. With reference to Fig. 5, to generate 3-DOF motions, two pairs of stator coils are required. From the figure, stator coils **S1**, **S2**, **S3**, and **S4** constitute the actuating elements of the spherical actuator. By the universal attraction law between unlike poles, forces will be generated upon activation of the stator coils. These forces are denoted by **F1**, **F2**, **F3**, and **F4**, resulting from energizing **S1**, **S2**, **S3**, and **S4**, respectively. Correspondingly, the figure also shows

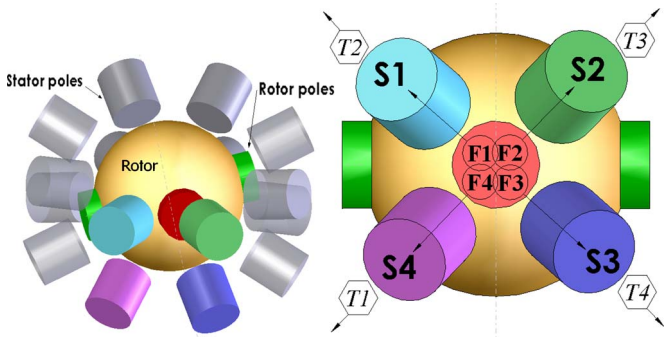

Fig. 5. Actuation strategy for 3-DOF motions.

TABLE I
PARAMETERS OF PROPOSED ELECTROMECHANICAL MODEL

Parameter	Description
$\mathbf{P}_{\mathrm{r}(k)}$	Position vector of the k^{th} rotor pole
$\mathbf{P}_{\mathrm{s}(l)}$	Position vector of the l^{th} stator pole
$\mathbf{P}^{\mathrm{s}(l)}_{\mathrm{c}(i,j)}$	Position vector of the $(i,j)^{\mathrm{th}}$ coil of the l^{th} stator pole
$\mathbf{P}^{\mathrm{s}(l)}_{\mathrm{r}(k)\text{-}\mathrm{c}(i,j)}$	Position vector from the k^{th} rotor pole to the $(i,j)^{\mathrm{th}}$ coil of the l^{th} stator pole
$\mathbf{B}^{\mathrm{s}(l)}_{\mathrm{c}(i,j)}$	$\mathbf{B}$-field acting on $(i,j)^{\mathrm{th}}$ coil of the l^{th} stator pole
$I^{\mathrm{s}(l)}$	Input current of the l^{th} stator pole
$A^{\mathrm{s}(l)}_{\mathrm{c}(i,j)}$	Surface area of $(i,j)^{\mathrm{th}}$ coil of the l^{th} stator pole
$\mathbf{T}_{\mathrm{R}(l)}$	Torque acting on rotor by the l^{th} stator pole
$\mathbf{T}_{\mathrm{rotor}}$	Total resultant torque acting on rotor

the resultant torque about the center of the rotor by $\boldsymbol{T1}$, $\boldsymbol{T2}$, $\boldsymbol{T3}$, and $\boldsymbol{T4}$ in the same order. It is through the combination of torque $\boldsymbol{T1}$ to $\boldsymbol{T4}$ that 3-DOF motions are achieved. Hence, in order to control the spherical actuator, analyzing the output torque is of paramount importance. The resultant output torque on the rotor is in fact the summation of the respective torque induced by the individual stator coil. Therefore, torque formulation for a set of rotor and stator poles will suffice as the remaining sets can be modeled in the similar fashion with positional variation.

The strategy behind this torque formulation is to establish the torque induced on the individual energized coils under the influence of $\mathbf{B}$ field from the rotor pole. Thereafter, by summing the respective torque, we will acquire the resultant torque of the stator coil. Since the stator coils are the stationary part, whereas the rotor is the moving part, from the third law of motion, we are able to derive the resultant torque acting on the rotor.

According to the magnetic-dipole-moment principle, to compute the torque acting on a single current coil, we have

$$\mathbf{T}_1 = \mathbf{m}_1 \times \mathbf{B}_1 \tag{7}$$

where $\mathbf{m}_1 = I_1 A_1 \hat{\mathbf{n}}_1$ and $\mathbf{B}_1$ is the magnetic-flux density acting through the planar area of the coil. Table I summarizes the parameters employed for the proposed electromechanical model.

In our prototype design, rare-earth magnets play the role of the rotor poles providing the required $\mathbf{B}$ field for actuation. As the fields from these hard magnets are uniform and intense within close proximity from the surface, $\mathbf{B}_1$ is referenced from the center of the coil.

The magnetic-field distribution in space of the rotor and stator coils can be comprehensively described by an analytical magnetic-field model that we proposed in an earlier work [15]. With reference to Fig. 6, the position of the rotor and stator poles can be described by spherical coordinates, r, θ, and ϕ. As rotational motions are involved during operation, it is essential to define coordinate frame for the moving parts. Hence, we define the global stator frame as $\{\mathbf{XYZ}\}$, the local rotor pole frame as $\{x_{\mathrm{rotor}}\ y_{\mathrm{rotor}}\ z_{\mathrm{rotor}}\}$, and the stator coil frame as $\{x_{\mathrm{coil}}\ y_{\mathrm{coil}}\ z_{\mathrm{coil}}\}$. During the evaluation, we will employ the $\mathbf{Z}$–$\mathbf{Y}$–$\mathbf{X}$ Euler angles convention for the mapping between the local and global coordinate frames. Without loss of generality, position vector of rotor pole $\mathbf{P}_{\mathrm{r1}}$ is positioned along the $\mathbf{X}$-axis. An arbitrary position of stator coil, $\mathbf{P}_{\mathrm{c1}}$, can be expressed by its spherical coordinates parameters r_{c1}, θ_{c1}, and ϕ_{c1}. Assuming a single-layer stator coil made up of n number of coils, the individual position vector of each coil can be defined by its respective spherical coordinate parameters. Therefore, we obtain the following position vectors:

$$\mathbf{P}_{\mathrm{r1}} = r_{r1}\begin{pmatrix}\cos\phi_{r1}\sin\theta_{r1}\\ \sin\phi_{r1}\sin\theta_{r1}\\ \cos\theta_{r1}\end{pmatrix}$$

$$\mathbf{P}_{\mathrm{c1}} = r_{c1}\begin{pmatrix}\cos\phi_{c1}\sin\theta_{c1}\\ \sin\phi_{c1}\sin\theta_{c1}\\ \cos\theta_{c1}\end{pmatrix} \cdots \mathbf{P}_{\mathrm{cn}} = r_{c(n)}\begin{pmatrix}\cos\phi_{c(n)}\sin\theta_{c(n)}\\ \sin\phi_{c(n)}\sin\theta_{c(n)}\\ \cos\theta_{c(n)}\end{pmatrix}. \tag{8}$$

When current is passed through the stator coil, the torque induced will attempt to align the coil with the $\mathbf{B}$ field from the rotor pole. This is analogous to the alignment of a magnetized needle with the Earth's magnetic field mentioned previously. Hence, the trajectory path that the rotor will undertake in order to minimize its potential energy will be the shortest path between the axial axis of the rotor $\mathbf{P}_{\mathrm{r1}}$ and stator pole $\mathbf{P}_{\mathrm{c1}}$. We define this shortest path between the two interacting element as $\mathbf{P}_{\mathrm{r1-c1}}$ as shown in Fig. 7

$$\mathbf{P}_{\mathrm{r1-c1}} = \mathbf{P}_{\mathrm{c1}} - \mathbf{P}_{\mathrm{r1}}. \tag{9}$$

Subsequently, by acquiring the magnetic-flux density $\mathbf{B}_1$ acting on coil C_1, we compute the torque at coil C_1 by the following:

$$\mathbf{T}_1 = I_1 A_1 (\hat{\mathbf{n}}_1 \times \mathbf{B}_1) \tag{10}$$

where I_1 is the current passing through the stator coil, $\hat{\mathbf{n}}_1$ is the unit normal vector along the coil axial axis, A_1 is the surface area of the loop, and $\mathbf{B}_1$ is the magnetic-flux density at the center of coil C_1. The accompanying advantage of using the magnetic-dipole-moment approach can be clearly seen from the fact that there are only two varying parameters, A_1 and $\mathbf{B}_1$ in the torque formulation with the remaining inputs as constants. In addition, with only one parameter being a vector and the other a scalar, inherent benefit will be the reduction

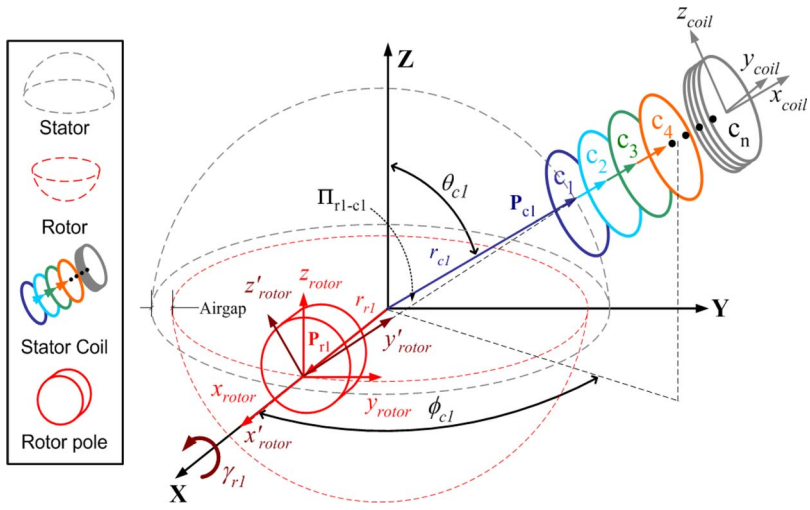

Fig. 6. Schematic of a set of rotor and stator poles.

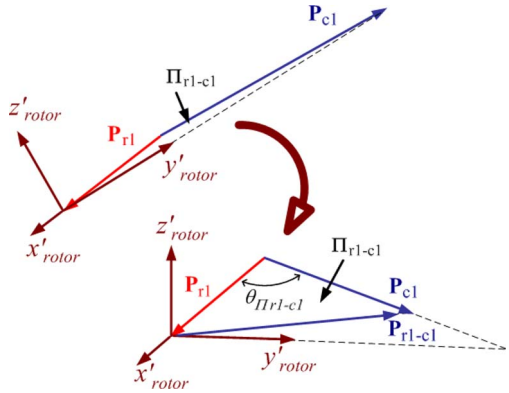

Fig. 7. Illustration of shortest path between rotor and stator poles.

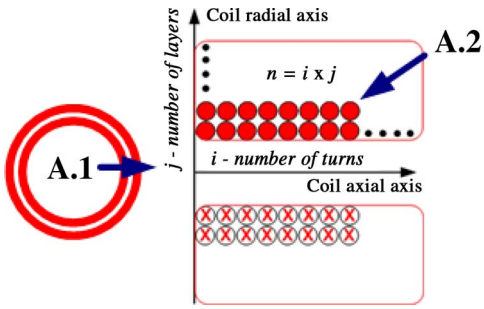

Fig. 8. Position vectors for $\mathbf{B}$-field calculation on rotated plane $\Pi_{\mathrm{r1-c1}}$.

of computational steps and time. What we have shown so far is the torque derivation for a single coil within a stator pole that comprises of n number of coils. Extending the same approach and summing up all the individual coils within the stator pole, we will be able to determine the resultant torque on the rotor induced by the input current into the coils. This notion is encapsulated as shown in Fig. 8. Therefore, we have the resultant torque as

$$\begin{aligned}\mathbf{T}_{\mathrm{R}} &= T_{\mathrm{c}(1,1)} + \mathbf{T}_{\mathrm{c}(1,2)} + \cdots + \mathbf{T}_{\mathrm{c}(i,j)} \\ &= \sum_{\mathrm{j}=1}^{\mathrm{j}} \sum_{\mathrm{i}=1}^{\mathrm{i}} \mathbf{T}_{\mathrm{c(i,j)}} \end{aligned} \tag{11}$$

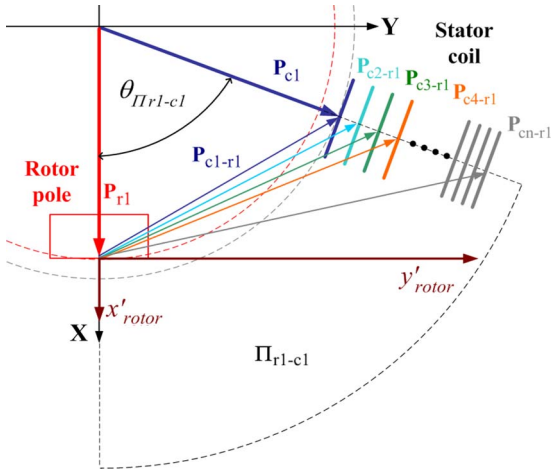

Fig. 9. Cross-sectional view of stator coil.

where i indicates the ith turn and j denotes the jth layer of the stator coil comprising of $n = i \times j$ number of turns as shown in Fig. 9 along with the following assumptions.

A.1) Current loop is assumed to be planar with respect to the coil axial axis.

A.2) Current loops are adjacent to each other with no overlap.

Henceforth, we have expounded on the conceptual idea and philosophy behind the proposed electromechanical model and its derivation process for the spherical actuator. As highlighted, motion generation of this type of spherical actuators can be achieved by a single pair of rotor and stator poles. As the input parameters are expressed in vectorial form in terms of its position vectors, we can conveniently include additional poles into this existing electromechanical model and acquire its total resultant torque consequently.

Since the fundamental configuration for 3-DOF motion generation require a set of four stator poles and one rotor pole, we can establish the full electromechanical model based on the extension of the prescribed basic arrangement and obtain the resultant as follows:

$$\mathbf{T}_{\mathrm{rotor}} = \mathbf{T}_{\mathrm{R1}} + \mathbf{T}_{\mathrm{R2}} + \mathbf{T}_{\mathrm{R3}} + \mathbf{T}_{\mathrm{R4}}. \tag{12}$$

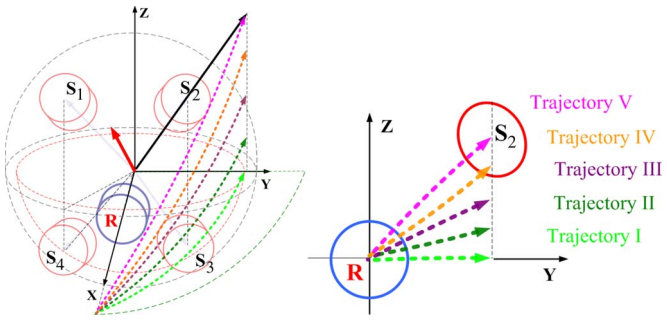

Fig. 10. Trajectories of test cases.

Equivalently, without any loss in generality, for l number of stator poles, we have

$$\mathbf{T}_{\text{rotor}} = \sum_{l=1}^{l} \mathbf{T}_{\text{R}(l)}. \tag{13}$$

The newly formulated analytical electromechanical model for the spherical actuator can be utilized for design optimization with respect to a given criterion. From the prototype-design aspect, the proposed electromechanical model is a function of the following parameters:

$$\mathbf{T}_{\text{rotor}} = f(I_{\text{stator}}, r_{\text{stator}}, t_{\text{stator}}, n_{\text{stator}} \times \theta_{\text{stator}}, \phi_{\text{stator}}, r_{\text{rotor}}, \theta_{\text{rotor}}, \phi_{\text{rotor}})$$

where

- I_{stator} input current;
- r_{stator} radial distance from rotor center to stator-pole surface;
- t_{stator} wire thickness;
- n_{stator} total of number of turns in stator pole;
- θ_{stator} stator-pole polar angle from the **Z**-axis;
- ϕ_{stator} stator-pole azimuthal angle in the **X**–**Y** plane from the **X**-axis;
- r_{rotor} radial distance from rotor center to rotor-pole surface;
- θ_{rotor} rotor-pole polar angle from the Z-axis;
- ϕ_{rotor} rotor-pole azimuthal angle in the **X**–**Y** plane from the **X**-axis.

IV. Validation of Electromechanical Model

In order to validate the theory behind the newly proposed electromechanical model, comparison will be drawn against the results generated from a numerical model and experimental investigations. The method of experiment is to subject the rotor **R** under five different trajectory paths (I–V) within the workspace of this spherical actuator as shown in Fig. 10. Along each path, resultant torque of the rotor will be computed by the proposed analytical and numerical models, with the empirical results acquired from the experimental setup as shown in Fig. 12. The objective is to collate all three sets of data and compare the results in order to authenticate the validity of the proposed analytical model.

Since this is a 3-DOF actuator, we shall investigate the workspace within the reachable range of our prototype along the trajectories as shown in Fig. 10. For each trajectory path, the rotor **R** will commence from the origin ($\phi = 0°$, $\theta = 90°$) and terminate at the respective azimuthal and polar angles specified in Table II. Along each trajectory, we discretize the path evenly for evaluation. In this case study, torque computation and measurement is based on the configuration between a cylindrical $\oslash$ 20 × 10-mm NdFeB rotor pole **R** and a $\oslash$ 20 × 20-mm stator coil $\mathbf{S}_2$ energized with an input current of 2 A as shown in Fig. 10.

TABLE II
Trajectories Position Angles

Parameter	Azimuthal angle, $\phi°$	Polar angle, $\theta°$
R	0	90
$\mathbf{S}_2$	30	70
Trajectory I	30	90
Trajectory II	30	85
Trajectory III	30	80
Trajectory IV	30	75
Trajectory V	30	70

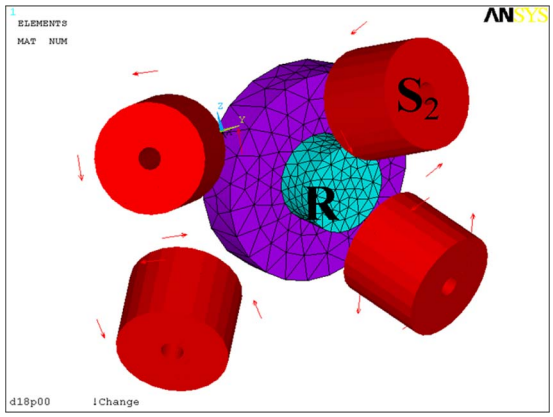

Fig. 11. Three-dimensional numerical model.

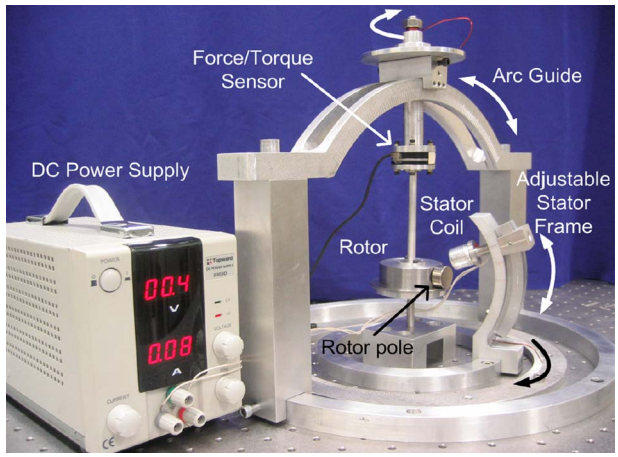

Fig. 12. Experimental setup for torque measurement.

A. Numerical Model

A 3-D finite-element model of the spherical actuator prototype was constructed using *ANSYS* for electromechanical and magnetic-field analyses as shown in Fig. 11. It is a replica of the physical system as shown in Fig. 10.

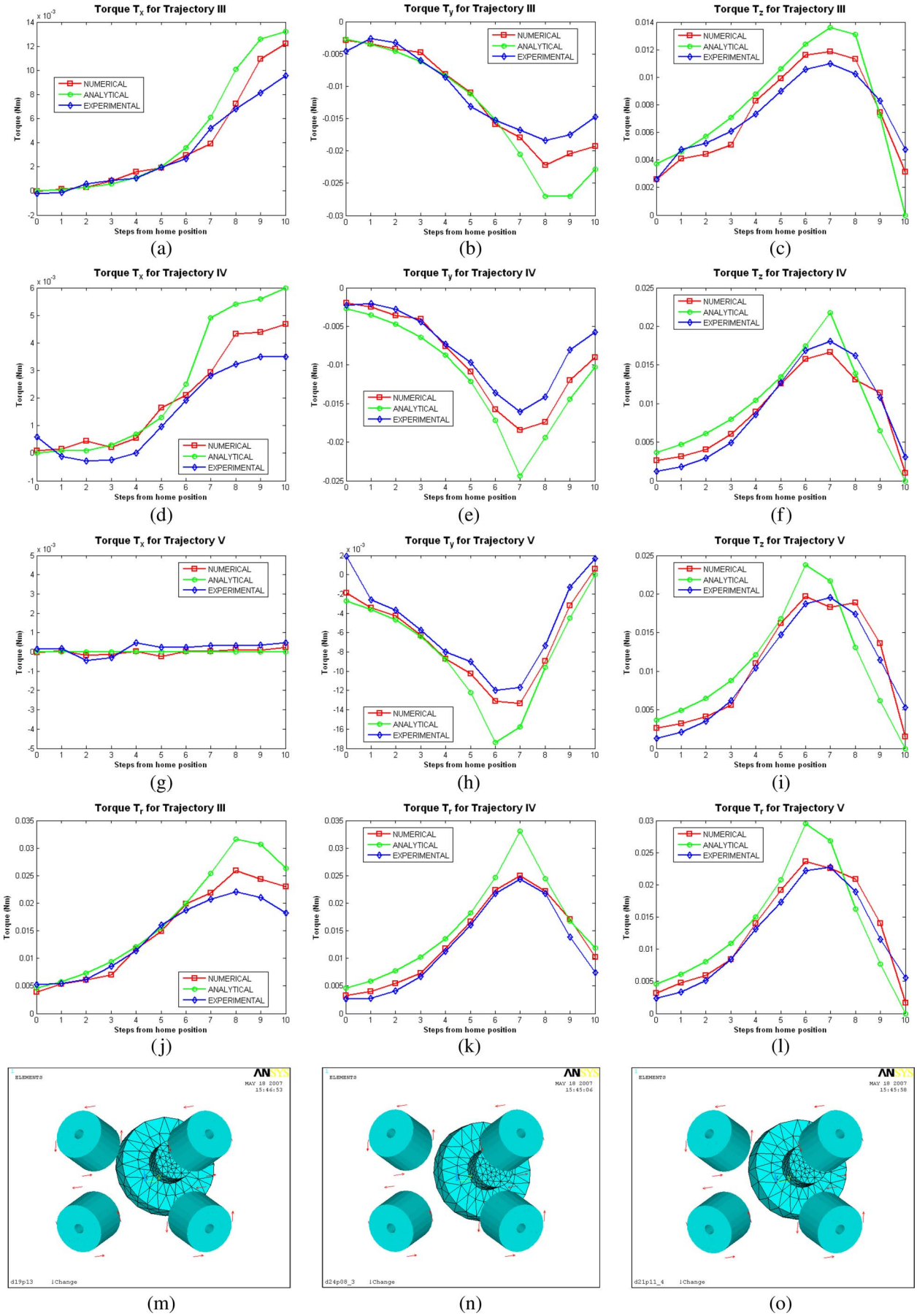

Fig. 13. Comparison of torque about principal axes between numerical, analytical, and empirical models.

From the formulated numerical model, trajectory paths I–V can be simulated by moving the rotor $\mathbf{R}$ along the respective trajectory. The resultant torque on the rotor will then be computed and compared with the analytical and empirical counterparts.

B. Experimental Setup

Experimental investigation was conducted using a skeleton model of the actual prototype as shown in Fig. 12. This experimental setup allows manipulation of various configurations and positions of both rotor and stator poles. Output torque measurement of the rotor can be acquired at different stator-pole positions by the six-axis force/torque sensor. Henceforth, the rotor will be subjected to the same trajectory paths stipulated in Table II, and resultant rotor torque will be registered by the force/torque sensor for subsequent comparisons. Fig. 13 shows a graphical summary of the torque generated by all models. Resultant torque about the $\mathbf{X}$-, $\mathbf{Y}$-, and $\mathbf{Z}$-axes are denoted by $\mathbf{T}_{\mathrm{x}}$, $\mathbf{T}_{\mathrm{y}}$, and $\mathbf{T}_{\mathrm{z}}$ with the corresponding plots for Trajectory III [Fig. 13(a)–(c)], Trajectory IV [Fig. 13(d)–(f)], and Trajectory V [Fig. 13(g)–(i)]. Based on these sets of results, we are able to draw the following observations.

1) The trend lines of $\mathbf{T}_{\mathrm{x}}$, $\mathbf{T}_{\mathrm{y}}$, and $\mathbf{T}_{\mathrm{z}}$ computed by the numerical and analytical models along with the acquired empirical results exhibit identical torque profile. The accuracy of the analytical model in comparison with the empirical data is observed to be < 0.01 Nm.
2) The correctness and reliability of the proposed analytical model is evidently authenticated by the profile of $\mathbf{T}_{\mathrm{x}}$. By comparing torque $\mathbf{T}_{\mathrm{x}}$ deduced from the analytical model along trajectories I–V, we observe a decreasing trend with trajectory path V showing $\mathbf{T}_{\mathrm{x}} = 0$ along that path. This occurrence can be rationalized as Trajectory V is along the shortest path between the rotor $\mathbf{R}$ and stator pole $\mathbf{S}_2$. Hence, with only $\mathbf{S}_2$ being energized, there should be no resultant torque on that particular axis. This is clearly reflected from the plot of $\mathbf{T}_{\mathrm{x}}$ of Trajectory V.
3) The analytical electromechanical model is able to accurately identify the maximum torque achievable. Maximum torque will occur when the stator pole experiences the highest magnetic-field density acting onto it. Geometrically, this coincides at positions when the rotor pole is nearing to the stator-pole surface. At the circumference or edge of the cylindrical poles, the fringing $\mathbf{B}$ field changes direction abruptly. Therefore, at the position where the edge of the rotor pole nears the stator pole, the torque will be the maximum. Beyond the position of maximum torque, the $\mathbf{B}$ field decreases and so will be the resulting induced torque. Fig. 13(j)–(o) shows the plot of the resultant torque $\mathbf{T}_{\mathrm{r}}$ of Trajectories III, IV, and V. As shown in Fig. 13(j)–(l), the peak of the torque curve from the analytical model increases as it nears the stator pole and equates to zero when it is fully aligned with the axis of stator pole $\mathbf{S}_2$. The finite-element model shown in Fig. 13(m)–(o) depicts the occurrence and indicates the exact position of this maximum torque for the respective trajectories.

V. Conclusion

From the preceding sections of this paper, we have proposed, reviewed, and assessed the validity of a new electromechanical model for PM spherical actuator based on the magnetic-dipole-moment principle. The advantages of our proposed model are as follows.

1) An analytical mathematical model correlating input and output parameters for direct computation of the induced resultant rotor torque in 3-D space. Inverse torque model can also be established from this approach.
2) The proposed approach distinguishes itself from existing conventional methods as torque is computed at current loop level, resulting in faster computational time essential and critical for real-time control.
3) Based on the magnetic-dipole-moment principle, this vectorial approach circumvents the need to conduct magnetic energy, field analysis, or integration which inherently is computationally exhaustive particularly in 3-D space.

The analytical model was verified with numerical and empirical results when the rotor was subjected to various trajectory paths. Comparison of the computed results by both approaches attests to the validity behind the analytical electromechanical model. The torque variation about three principle axes deduced by the proposed model maps the same torque profile as compared to the numerical and empirical counterparts, the soundness of the theory behind the newly formulated electromechanical model. Moreover, geometric interpretation of the torque curve with the position of the rotor at maximum torque reinforces the soundness of the theory behind the newly formulated electromechanical model.

In conclusion, the analytical model proposed in this paper was validated by its corresponding numerical model and empirical data with results showing good fit between them. This novel approach using magnetic dipole moment to describe and determine resultant torque of PM spherical actuator has been verified in principle, and this brings a new dimension to the analysis, design optimization, and control of such class of actuators.

References

[1] F. Williams, E. Laithwaite, and L. Piggot, "Brushless variable speed induction motor," *Proc. Inst. Electr. Eng.*, vol. 104A, no. 2097U, pp. 102–118, Jun. 1956.
[2] G. J. Vachtsevanos, K. Davey, and K. M. Lee, "Development of a novel intelligent robotic manipulator," *IEEE Control Syst. Mag.*, vol. 7, no. 3, pp. 9–15, Jun. 1987.
[3] K. Davey, G. Vachtsevanos, and R. Powers, "The analysis of fields and torques in spherical induction motors," *IEEE Trans. Magn.*, vol. MAG-23, no. 1, pp. 273–282, Jan. 1987.
[4] K. Kaneko, I. Yamada, and K. Itao, "A spherical DC servo motor with three degrees of freedom," *Trans. ASME, J. Dyn. Syst. Meas. Control*, vol. 111, pp. 433–443, 1988.
[5] K. M. Lee and C. K. Kwan, "Design concept development of a spherical stepper for robotics applications," *IEEE Trans. Robot. Autom.*, vol. 7, no. 1, pp. 175–181, Feb. 1991.
[6] S. Toyama, S. Hatae, and M. Nonaka, "Development of multi-degree of freedom spherical ultrasonic motor," in *Proc. 5th Int. Conf. Advanced Robot.*, 1991, pp. 55–60.
[7] C. I. Yang and Y. S. Baek, "Design and control of the 3 degrees of freedom actuator by controlling the electromagnetic force," *IEEE Trans. Magn.*, vol. 35, no. 5, pp. 3607–3609, Sep. 1999.
[8] G. S. Chirikjian and D. Stein, "Kinematic design and commutation of a spherical stepper motor," *IEEE/ASME Trans. Mechatronics*, vol. 4, no. 4, pp. 342–353, Dec. 1999.

[9] H. Nagasawa and S. Honda, "Development of a spherical motor manipulated by four wires," in *Proc. 15th Annu. Meeting Amer. Soc. Precision Eng.*, 2000, vol. 22, pp. 219–222.
[10] J. Wang, G. W. Jewell, and D. Howe, "Analysis, design and control of a novel spherical permanent-magnet actuator," *Proc. Inst. Elect. Eng.—Elect. Power Appl.*, vol. 145, no. 1, pp. 61–71, Jan. 1998.
[11] C. K. Lim, L. Yan, I-M. Chen, G. L. Yang, and W. Lin, "Mechanical design & numerical electromagnetic analysis of a DC spherical actuator," in *Proc. IEEE Int. Conf. Robot., Autom. Mechatronics*, Dec. 2004, vol. 1, pp. 536–541.
[12] B. Dehez, G. Galary, D. Grenier, and B. Raucent, "Development of a spherical induction motor with two degrees of freedom," *IEEE Trans. Magn.*, vol. 42, no. 8, pp. 2077–2089, Aug. 2006.
[13] K. M. Lee and H. Son, "Distributed multipole model for design of permanent-magnet-based actuators," *IEEE Trans. Magn.*, vol. 43, no. 10, pp. 3904–3913, Oct. 2007.
[14] J. Wang, W. Wang, G. W. Jewell, and D. Howe, "Design of a miniature permanent-magnet generator and energy storage system," *IEEE Trans. Ind. Electron.*, vol. 52, no. 5, pp. 1383–1390, Oct. 2005.
[15] C. K. Lim and I-M. Chen, "Magnetic field modeling of a permanent magnet electromagnetic spherical actuator," in *Proc. 17th CISM-IFToMM RoManSy*, Jul. 5–9, 2008, pp. 561–570.
[16] L. Yan, I-M. Chen, C. K. Lim, G. L. Yang, W. Lin, and K. M. Lee, "Design and analysis of a permanent magnet spherical actuator," *IEEE/ASME Trans. Mechatronics*, vol. 13, no. 2, pp. 239–248, Apr. 2008.
[17] P. Pillay and R. Krishnan, "Modeling of permanent magnet motor drives," *IEEE Trans. Ind. Electron.*, vol. 35, no. 4, pp. 537–541, Nov. 1988.
[18] M. L. Graham and S. Gruber, "Simulation study of an electronically commutated DC machine," *IEEE Trans. Ind. Electron.*, vol. IE-32, no. 4, pp. 399–405, Nov. 1985.
[19] L. Parsa and L. Hao, "Interior permanent magnet motors with reduced torque pulsation," *IEEE Trans. Ind. Electron.*, vol. 55, no. 2, pp. 602–609, Feb. 2008.
[20] J. Cheol, J. Y. Seol, and I. J. Ha, "Flux-weakening control of IPM motors with significant effect of magnetic saturation and stator resistance," *IEEE Trans. Ind. Electron.*, vol. 55, no. 3, pp. 1330–1340, May 2008.

Chee Kian Lim received the M.Eng. and Ph.D. degrees in mechanical engineering from Nanyang Technological University, Singapore, in 2001 and 2008, respectively.

He is currently a Research Fellow with Nanyang Technological University, where he is working on ultrasonic motors in the School of Mechanical and Aerospace Engineering. He was a National Science and Technology Board and Agency for Science, Technology and Research (A*STAR) scholar during his undergraduate and postgraduate studies. His fields of research are smart actuators, system design, and modeling.

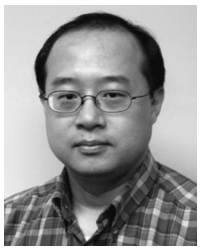

I-Ming Chen (SM'06) received the B.S. degree from National Taiwan University, Taipei, Taiwan, in 1986, and the M.S. and Ph.D. degrees from California Institute of Technology, Pasadena, in 1989 and 1994, respectively.

Since 1995, he has been with the School of Mechanical and Aerospace Engineering, Nanyang Technological University (NTU), Singapore, where he is currently the Director of the Intelligent Systems Center, a partnership between Singapore Technology Engineering Ltd. and NTU. He was a JSPS Visiting Scholar at Kyoto University, Kyoto, Japan, in 1999, and a Visiting Scholar in the Department of Mechanical Engineering, Massachusetts Institute of Technology (MIT), Cambridge, in 2004. He is currently a Fellow of the Singapore–MIT Alliance under the Manufacturing Systems and Technology Program. He has published more than 170 technical articles in refereed international journals and conference proceedings. His research interests include wearable sensors, human–robot interaction, novel actuator design, reconfigurable automation, parallel kinematics machines, and biomorphic underwater robots.

Dr. Chen is a member of the American Society of Mechanical Engineers (ASME) and a member of the RoboCup Singapore National Committee. He is currently serving on the Editorial Boards of the IEEE TRANSACTIONS ON ROBOTICS and the IEEE/ASME TRANSACTIONS ON MECHATRONICS and *Robotica*. He is the General Chairman of the 2009 IEEE/ASME International Conference on Advanced Intelligent Mechatronics (AIM2009) in Singapore.

Liang Yan (M'07) received the B.Eng. degree from North China Institute of Science and Technology, Beijing, China, in 1995, the M.Eng. degree from Beijing Institute of Technology, Beijing, in 1998, and the Ph.D. degree from Nanyang Technological University, Singapore, in 2007.

From 1998 to 2002, he was a Lecturer with Beijing Institute of Technology. He is currently with the School of Mechanical and Aerospace Engineering, Nanyang Technological University. His research interests include electromagnetic actuators, sensors, navigation system, and expert system design.

Dr. Yan is the Publication Chairman of the 2008 IEEE International Conference on Cybernetics and Intelligent Systems and the 2008 IEEE International Conference on Robotics, Automation and Mechatronics. He was the recipient of the National Defense Science and Technology Award of China in 2002.

Guilin Yang (M'02) received the B.Eng. and M. Eng. degrees from Jilin University of Technology (currently Jilin University), Changchun, China, in 1985 and 1988, respectively, and the Ph.D. degree from Nanyang Technological University, Singapore, in 1999.

In 1988, he was with the School of Mechanical Engineering, Shijiazhuang Railway Institute, Shijiazhuang, China, where he was a Lecturer, a Division Head, and then the Vice Dean of the school, for nearly seven years. He is currently a Research Scientist and the Group Manager with the Mechanics Group, Singapore Institute of Manufacturing Technology, Singapore. He has published over 130 technical papers in refereed journals and conference proceedings. His current research interests include computational kinematics, multibody dynamics, parallel-kinematics machines, modular robots, flexure-based precision mechanisms, electromagnetic actuators, rehabilitation devices, and industrial robotic systems.

Dr. Yang is a Technical Committee Member of the Robotics of International Federation for the Promotion of Mechanism and Machine Science, the Deputy Chair of the Singapore Chapter of the IEEE Robotics and Automation Society, and a Technical Editor for the IEEE/ASME TRANSACTIONS ON MECHATRONICS.

Kok-Meng Lee (M'89–SM'02–F'05) received the M.S. and Ph.D. degrees in mechanical engineering from Massachusetts Institute of Technology, Cambridge, in 1982 and 1985, respectively.

Since 1985, he has been with the Faculty of Mechanical Engineering, Georgia Institute of Technology, Atlanta, where he is currently a Professor. He is the holder of seven patents. His current research interests include system dynamics and control, machine vision, robotics, automation, and mechatronics.

Dr. Lee is a Fellow of the American Society of Mechanical Engineers. He has served on representative positions within the IEEE Robotics and Automation Society (RAS). He was an Associate Editor of the IEEE TRANSACTIONS ON ROBOTICS AND AUTOMATION from 1994 to 1998, the *IEEE Robotic and Automation Magazine* from 1994 to 1996, and the IEEE TRANSACTIONS ON AUTOMATION AND ENGINEERING from 2003 to 2005 and a Technical Editor of the IEEE/ASME TRANSACTIONS ON MECHATRONICS from 1995 to 1999. Since 2008, he has been the Editor-in-Chief for the IEEE/ASME TRANSACTIONS ON MECHATRONICS. He was the recipient of numerous awards including the NSF Presidential Young Investigator (PYI) Award, Sigma Xi Junior Faculty Award, International Hall of Fame New Technology Award, Woodruff Faculty Fellow, and three Best Paper Awards. He is also recognized as an Advisor for seven Best Student Paper Awards and a Best Thesis Award.